Oxygen partial pressure dependence of magnetic, optical and magneto-optical properties of epitaxial cobalt-substituted $SrTiO_3$ films

Mehmet C. Onbaşlı,[1] Taichi Goto,[2] Astera Tang,[1] Annia Pan,[1] Enes Battal,[3] Ali K. Okyay,[3,4] Gerald F. Dionne,[1] C. A. Ross[1,*]

[1]*Department of Materials Science and Engineering, Massachusetts Institute of Technology, 77 Masshuchusetts Avenue, MIT Cambridge, MA 02139 USA*

[2]*Department of Electrical and Electronic Information Engineering, Toyohashi University of Technology, 1-1 Hibarigaoka, Tempaku, Toyohashi, Aichi 441-8580, Japan*

[3]*Department of Electrical and Electronics Engineering, Bilkent University, Ankara 06800, Turkey*

[4]*UNAM, Institute of Materials Science and Nanotechnology, Bilkent University, Ankara 06800, Turkey*

[*]*caross@mit.edu*

Abstract: Cobalt-substituted $SrTiO_3$ films ($SrTi_{0.70}Co_{0.30}O_{3-\delta}$) were grown on $SrTiO_3$ substrates using pulsed laser deposition under oxygen pressures ranging from 1 μTorr to 20 mTorr. The effect of oxygen pressure on structural, magnetic, optical, and magneto-optical properties of the films was investigated. The film grown at 3 μTorr has the highest Faraday rotation (FR) and magnetic saturation moment (M_s). Increasing oxygen pressure during growth reduced M_s, FR and optical absorption in the near-infrared. This trend is attributed to decreasing Co^{2+} ion concentration and oxygen vacancy concentration with higher oxygen partial pressure during growth.

OCIS codes: (160.3820) Magneto-optical materials; (240.0310) Thin films; (310.1860) Deposition and fabrication; (310.3840) Materials and process characterization.

References and links

1. M. Cardona, "Optical Properties and Band Structure of $SrTiO_3$ and $BaTiO_3$," Phys. Rev. **140**(2A), A651–A655 (1965).
2. K. van Benthem, C. Elsässer, and R. H. French, "Bulk electronic structure of $SrTiO_3$: Experiment and theory," J. Appl. Phys. **90**(12), 6156 (2001).
3. L. Bi, H. S. Kim, G. F. Dionne, and C. A. Ross, "Structure, magnetic properties and magnetoelastic anisotropy in epitaxial $Sr(Ti_{1-x}Co_x)O_3$ films," New J. Phys. **12**(4), 043044 (2010).
4. M. Gaidi, L. Stafford, J. Margot, M. Chaker, R. Morandotti, and M. Kulishov, "Microfabricated $SrTiO_3$ ridge waveguides," Appl. Phys. Lett. **86**(22), 221106 (2005).
5. G. Herranz, R. Ranchal, M. Bibes, H. Jaffrès, E. Jacquet, J. L. Maurice, K. Bouzehouane, F. Wyczisk, E. Tafra, M. Basletic, A. Hamzic, C. Colliex, J. P. Contour, A. Barthélémy, and A. Fert, "Co-doped (La, Sr)$TiO_{3-\delta}$: a high Curie temperature diluted magnetic system with large spin polarization," Phys. Rev. Lett. **96**(2), 027207 (2006).
6. X. S. Zhang, W. Yu, S. B. Ogale, S. R. Shinde, D. C. Kundaliya, W. Tse, S. Y. Young, J. S. Higgins, L. G. Salamanca-Riba, M. Herrera, L. F. Fu, N. D. Browning, R. L. Greene, and T. Venkatesan, "Magnetism and anomalous Hall effect in Co-(La,Sr)TiO_3," Phys. Rev. B **76**(8), 085323 (2007).
7. P. Plonczak, A. Bieberle-Hutter, M. Sogaard, T. Ryll, J. Martynczuk, R. V. Hendriksen, and L. J. Gauckler, "Tailoring of $La_xSr_{1-x}Co_yFe_{1-y}O_{3-\delta}$ Nanostructure by Pulsed Laser Deposition," Adv. Funct. Mater. **21**(14), 2764–2775 (2011).
8. H. S. Kim, L. Bi, G. F. Dionne, and C. A. Ross, "Magnetic and magneto-optical properties of Fe-doped $SrTiO_3$ films," Appl. Phys. Lett. **93**(9), 092506 (2008).
9. D. H. Kim, L. Bi, P. Jiang, G. F. Dionne, and C. A. Ross, "Magnetoelastic effects in $SrTi_{1-x}M_xO_3$ (M = Fe, Co, or Cr) epitaxial thin films," Phys. Rev. B **84**(1), 014416 (2011).
10. P. Jiang, L. Bi, X. Sun, D. H. Kim, D. Jiang, G. Wu, G. F. Dionne, and C. A. Ross, "The effect of A-site substitution of Ce and La on the magnetic and electronic properties of $Sr(Ti_{0.6}Fe_{0.4})O_{3-\delta}$ films," Inorg. Chem. **51**(24), 13245–13253 (2012).
11. D. H. Kim, L. Bi, N. M. Aimon, P. Jiang, G. F. Dionne, and C. A. Ross, "Combinatorial pulsed laser deposition of Fe, Cr, Mn, and Ni-substituted $SrTiO_3$ films on Si substrates," ACS Comb Sci **14**(3), 179–190 (2012).

#234231 - $15.00 USD Received 9 Feb 2015; accepted 30 Apr 2015; published 13 May 2015

12. H. Dötsch, N. Bahlmann, O. Zhuromskyy, M. Hammer, L. Wilkens, R. Gerhardt, and P. Hertel, "Applications of magneto-optical waveguides in integrated optics: review," J. Opt. Soc. Am. B **22**, 240 (2005).
13. L. Bi, J. Hu, P. Jiang, D. H. Kim, G. F. Dionne, L. C. Kimerling, and C. A. Ross, "On-chip optical isolation in monolithically integrated non-reciprocal optical resonators," Nat. Photonics **5**(12), 758–762 (2011).
14. G. F. Dionne, L. Bi, H.-S. Kim, and C. A. Ross, "Spectral origins of high Faraday rotation at 1.5-μm wavelength from Fe and Co in $SrTiO_3$ films," J. Appl. Phys. **109**(7), 07B761 (2011).
15. G. F. Dionne, D. H. Kim, L. Bi, and C. A. Ross, "Generic model of superexchange effects in magnetoelastic oxides," J. Appl. Phys. **113**(17), 17A927 (2013).
16. G. F. Dionne, A. Taussig, M. Bolduc, L. Bi, and C. A. Ross, "Mixed-cation designs of magnetic perovskites for Faraday rotation at IR wavelengths," J. Appl. Phys. **101**(9), 09C524 (2007).
17. H. S. Kim, L. Bi, H. Paik, D. J. Yang, Y. C. Park, G. F. Dionne, and C. A. Ross, "Self-assembled single-phase perovskite nanocomposite thin films," Nano Lett. **10**(2), 597–602 (2010).
18. J. M. Florez, S. P. Ong, M. C. Onbasli, G. F. Dionne, P. Vargas, G. Ceder, and C. A. Ross, "First-principles insights on the magnetism of cubic $SrTi_{1-x}Co_xO_{3-\delta}$," Appl. Phys. Lett. **100**(25), 252904 (2012).
19. Y. Guo, B. Guo, W. Dong, H. Li, and H. Liu, "Evidence for oxygen vacancy or ferroelectric polarization induced switchable diode and photovoltaic effects in $BiFeO_3$ based thin films," Nanotechnology **24**(27), 275201 (2013).
20. D. Kan, T. Terashima, R. Kanda, A. Masuno, K. Tanaka, S. Chu, H. Kan, A. Ishizumi, Y. Kanemitsu, Y. Shimakawa, and M. Takano, "Blue-light emission at room temperature from Ar^+-irradiated $SrTiO_3$," Nat. Mater. **4**(11), 816–819 (2005).
21. H. L. Ju, J. Gopalakrishnan, J. L. Peng, Q. Li, G. C. Xiong, T. Venkatesan, and R. L. Greene, "Dependence of giant magnetoresistance on oxygen stoichiometry and magnetization in polycrystalline $La_{0.67}Ba_{0.33}MnO_z$," Phys. Rev. B Condens. Matter **51**(9), 6143–6146 (1995).
22. P. Jiang, L. Bi, D. H. Kim, G. F. Dionne, and C. A. Ross, "Enhancement of the magneto-optical performance of $Sr(Ti_{0.6-x}Ga_xFe_{0.4})O_3$ perovskite films by Ga substitution," Appl. Phys. Lett. **98**(23), 231909 (2011).
23. T. Saitoh, T. Mizokawa, A. Fujimori, M. Abbate, Y. Takeda, and M. Takano, "Electronic structure and magnetic states in $La_{1-x}Sr_xCoO_3$ studied by photoemission and x-ray-absorption spectroscopy," Phys. Rev. B **56**(3), 1290–1295 (1997).
24. S. Malo and A. Maignan, "Structural, magnetic, and transport properties of the SrTi1-xCoxO3-δ perovskite (0 < or = x < or = 0.9)," Inorg. Chem. **43**(25), 8169–8175 (2004).
25. T. Nitadori, M. Muramatsu, and M. Misono, "Valence control, reactivity of oxygen, and catalytic activity of lanthanum strontium cobalt oxide ($La_{2-x}Sr_xCoO_4$)," Chem. Mater. **1**(2), 215–220 (1989).
26. L. Bi, "Magneto-optical Oxide Thin Films And Integrated Nonreciprocal Photonic Devices," PhD Thesis, Massachusetts Institute of Technology (2011).
27. H.-S. Kim, L. Bi, G. F. Dionne, and C. A. Ross, "Magnetic and magneto-optical properties of Fe-doped $SrTiO_3$ films," Appl. Phys. Lett. **93**(9), 092506 (2008).
28. T. Goto, Y. Eto, K. Kobayashi, Y. Haga, M. Inoue, and C. A. Ross, "Vacuum annealed cerium-substituted yttrium iron garnet films on non-garnet substrates for integrated optical circuits," J. Appl. Phys. **113**(17), 17A939 (2013).
29. S. Higuchi, Y. Furukawa, S. Takekawa, O. Kamada, and K. Kitamura, "Magneto-optical properties of Cerium-Substituted Yttrium iron garnet single crystals grown by traveling solvent floating zone method," Jpn. J. Appl. Phys. **38**(Part 1, No. 7A), 4122–4126 (1999).
30. T. Shintaku, "Integrated optical isolator based on efficient nonreciprocal radiation mode conversion," Appl. Phys. Lett. **73**(14), 1946 (1998).
31. T. R. Zaman, X. Guo, and R. J. Ram, "Faraday rotation in semiconductors for photonic integration," in Proc. Conf. Lasers Electro-Optics, San Francisco, CA, May 2004, p. 2.
32. T. R. Zaman, X. Guo, and R. J. Ram, "Faraday rotation in an InP waveguide," Appl. Phys. Lett. **90**(2), 023514 (2007).

1. Introduction

$SrTiO_3$ (STO) is a functional wide band gap perovskite (indirect E_g = 3.2 eV) that is transparent to optical and near-infrared telecommunication wavelengths [1,2]. STO is highly transparent near λ = 1.55 μm in thin film and waveguide forms [3,4]. Transition metal substituted STO films, such as $Sr(Ti,Co)O_{3-\delta}$ [3], $(La,Sr)(Ti,Co)O_{3-\delta}$ [5–7], and $Sr(Ti,Fe)O_{3-\delta}$ (STF) [8–11], exhibit room temperature magnetic and magneto-optical (MO) properties which depend on substrate, substituent type and concentration, buffer layer and film growth conditions. Faraday rotation of substituted STO films make these films attractive for integrated non-reciprocal photonic device applications [12,13] such as isolators and circulators as well as for fundamental investigations of the spectral origins of MO properties and superexchange effects [9,14–16]. Substituted STO films can be grown both as polycrystalline films on Si or as single crystals on perovskite substrates, but on CeO_2/yttria-stabilized zirconia buffered Si, STF films grew with two different epitaxial orientations,

#234231 - $15.00 USD Received 9 Feb 2015; accepted 30 Apr 2015; published 13 May 2015

forming so-called double-epitaxial growth in which the (100)-oriented film contained (110) crystals which formed to relieve strain [17].

In an earlier study, the structural, magnetic and magneto-optical properties of $Sr(Ti,Co)O_{3-\delta}$ (STCo) films on $LaAlO_3$ substrates were characterized [3]. The lattice constant of the STCo films increased with Co concentration. STCo films showed in-plane compressive strain as well as a tetragonal unit cell with c-axis along the out-of-plane direction (*c/a* ~1.028 for Co 37.5%). Out-of-plane lattice parameter *c* increased by ~1.39% (3.960 to 4.015Å) as Co concentration was increased from 0% to 37.5%. As Co concentration increased, the magnetic moment increased for Co up to ~30% Co, then decreased. Saturation moments up to 0.5 μ_B per Co ion and an out-of-plane easy magnetization axis were observed at room temperature. Faraday rotations up to −500 deg·cm^{-1} at λ = 1550 nm were demonstrated. The MO hysteresis of these films also showed an out-of-plane easy magnetic axis, potentially useful for developing TE (transverse electric) mode non-reciprocal devices. At 1550 nm, the optical constants for STCo were n = 2.34 and k = 1.1 × 10^{-3} and the MO figure-of-merit (Faraday rotation, in units of deg·cm^{-1}, over optical loss, dB cm^{-1}) was 0.57 deg·dB^{-1}.

These results suggest that Co- or Fe-substituted STO may be useful in magneto-optical devices, though their MO performance to date is not as good as that of iron garnets. Ref. 3 indicated that the base pressure prior to deposition had a significant effect on the magnetic properties of STCo films, though this was not explored in depth. The base pressure during growth is expected to affect the oxygen vacancy concentration, altering properties such as optical absorption and magnetism [18]. Oxygen vacancies have many profound effects on perovskites, for instance, electromigration of oxygen vacancies was able to induce reversibly-switchable diode and photovoltaic effects in $Bi_{0.9}Sr_{0.1}FeO_{3-\delta}$ thin films [19]. Blue light was emitted from Ar^+-irradiated STO thin films due to radiative recombination of conduction electrons and holes stabilized within the band gap of STO [20]. In another study, the resistivity of $La_{0.67}Ba_{0.33}MnO_z$ was enhanced about four orders of magnitude at room temperature by reducing oxygen content from z = 2.99 to 2.80 [21]. The control of oxygen stoichiometry in perovskites opens the possibility of electrical control of carrier density, magnetic and MO functionalities, which could enable devices such as electrically controlled non-reciprocal photonic modulators.

In this study, cobalt-substituted STO thin films made from a target with 30 at.% Cobalt, or STCo30 hereafter, were grown on STO substrates under different oxygen pressures, and changes in their structural, magnetic, optical and MO properties as a function of oxygen pressure during growth were investigated. 30 at.% Co concentration was chosen since this concentration has been found to maximize magnetic moment and Faraday rotation [3]. In the following sections, first the growth procedure of the films is described, then the phase formation and ionic valence states are investigated. Magnetic properties are discussed in context of the mixed valence states of Cobalt ions. Finally, optical and MO properties of the films are studied, and growth conditions for STCo30 films with optimum MO figure-of-merit is presented.

2. PLD target preparation and film growth method

Precursor powders of $SrCO_3$, TiO_2 and CoO were mixed at the stoichiometric cation ratios of the final target composition ($SrTi_{0.70}Co_{0.30}O_{3-\Delta}$, oxygen deficiency of the target: Δ) and ball milled with alumina grinding media for 24 hours in ethanol. The mixture was then dried and calcinated for 12 hours in a tube furnace at 1400°C in air. Next, the calcinated powder was cold isostatically pressed (CIP) at 40,000 psi for 2 min into a 1" diameter disk. Finally, the disk was transferred to a tube furnace and sintered at 1400°C for 18 hours to form the final STCo30 target.

The films were prepared by pulsed laser deposition (PLD). Double-side polished, 10 mm x 10 mm area STO (001) substrates (MTI Crystals Inc.) were cleaned with ultra-sonication in acetone and then isopropanol for 10 minutes each. The substrates were loaded into the

#234231 - $15.00 USD Received 9 Feb 2015; accepted 30 Apr 2015; published 13 May 2015

chamber which was pumped down to $1x10^{-6}$ Torr base pressure. Assuming the base pressure gas contains about ~20% oxygen (atmospheric fraction of oxygen), the oxygen partial pressure before setting the oxygen flow is taken as $\sim 2x10^{-7}$ Torr. After reaching the base pressure at 23°C, the oxygen partial pressure was set manually using a mass flow control valve (attached to a pure oxygen cylinder) to the values indicated on Table 1.

Table 1. STCo sample list, structural, optical and MO properties.

Sample Name	Film Thickness (nm)	Out-of-plane lattice parameter (Å)	Lattice volume ($Å^3$)	Oxygen Pressure (Torr)	Faraday rotation at 1550 nm ($°\cdot cm^{-1}$)	Optical Loss at 1550 nm ($x10^3$) ($dB\cdot cm^{-1}$)	Figure-of-merit ($x10^{-3}$) ($°\cdot dB^{-1}$)
1 μTorr	270	3.956	60.33	$< 1x10^{-6}$	−75 ± 15	37.8 ± 1.8	1.99
3 μTorr	280	3.961	60.40	$< 3x10^{-6}$	−220 ± 10	23.6 ± 1.1	9.33
6 μTorr	281	3.931	59.94	$5x10^{-6}$	−80 ± 30	33.4 ± 1.6	2.39
9 μTorr	250	3.915	59.70	$8x10^{-6}$	−92 ± 20	6.8 ± 0.3	13.5
5mTorr	260	3.926	59.87	$5x10^{-3}$	−27 ± 10	14.2 ± 0.7	1.88
10mTorr	237	3.901	59.49	$1x10^{-2}$	−31 ± 5	21.1 ± 1.1	1.47
20mTorr	256	3.908	59.59	$2x10^{-2}$	−25 ± 10	0.390 ± 0.1	64

The substrate was then heated under constant oxygen pressure and the film was deposited by ablating the PLD target. A KrF excimer laser (λ = 248 nm, pulse duration 25 ns, pulse rate 10 Hz) was used to grow the films on STO substrates held at 650°C substrate temperature. The laser spot size on the target was 0.5 x 2.0 mm and the energy density at the target surface was ~1.3 J cm^{-2} during the pulse. The growth rate was 2.8 $nm\cdot min^{-1}$ for lower pressure samples (1-9 μTorr) and 1.76 $nm\cdot min^{-1}$ for higher oxygen pressure samples (5, 10 and 20mTorr). During depositions, the STCo30 target was rotated to improve uniformity in thickness and composition. A previous study indicates that the cation stoichiometry is $SrTi_{0.77}Co_{0.23}O_{3-\delta}$ [3] (oxygen deficiency of the film: δ). After deposition, the chamber was cooled at a rate of 5°C min^{-1}. Films with similar thicknesses were grown at the same processing conditions indicated on Table 1. 21 separate films were prepared (3 pieces per oxygen pressure) and a representative set was presented with error bars.

3. Structural and magnetic properties of STCo30 films

X-ray diffraction (XRD) was used to identify the phases within the STCo30 films and to extract the out-of-plane lattice parameters of films as a function of oxygen partial pressure. Figure 1(a) indicates the ω-2θ scans for STCo30 films near STO (200) substrate peak, measured using a PANalytical X'Pert PRO MPD X-ray diffractometer (Cu K_α radiation source at the wavelength of 0.1541 nm). During ω-2θ measurements, the substrates were not tilted in order to pick up the strong substrate peak and the film peaks at the same time. The bare substrate shows strong STO peaks at 2θ = 46.5° and additionally a small peak at 45.5° and a step at 44.8°. The STCo30 (200) peaks are found to the left of the STO peak, broader and lower intensity than the STO peak. A reciprocal space map measurement done on the STCo30 (1 μTorr)/STO sample (not shown) indicated that even when the films were about 200 nm thick, the in-plane lattice parameter of the films and the substrate were identical, therefore the films were epitaxial with the substrate. The surface roughness of the films was less than 2 nm peak-to-peak.

The out-of-plane lattice parameters were extracted from the ω-2θ scans and they are listed in Table 1, with error 0.005 Å. In some cases, e.g. 3 μTorr, the peak was split suggesting relaxation of part of the film, as seen in $Sr(Ti,Ga,Fe)O_{3-\delta}$ films [22]. The smaller out-of-plane

#234231 - $15.00 USD Received 9 Feb 2015; accepted 30 Apr 2015; published 13 May 2015

lattice parameter (less strained) was calculated in Table 1. The more strained fraction of the 3 μTorr film has 4.012Å for out-of-plane lattice parameter (2.7% strain on STO substrate, unit cell volume: a ·3.905^2 Å^2 = 61.18 Å^3). The films grown at lower oxygen partial pressures (1-9 μTorr films) had out-of-plane lattice parameters *c* larger than the in-plane lattice parameter of the STO substrates (*a* = 3.905 Å), i.e. the *c/a* ratio was up to 1.014 assuming the film is lattice matched to the substrate in plane. All films contained perovskite phases, but metallic Cobalt or Co oxide peaks were not observed for any of the films.

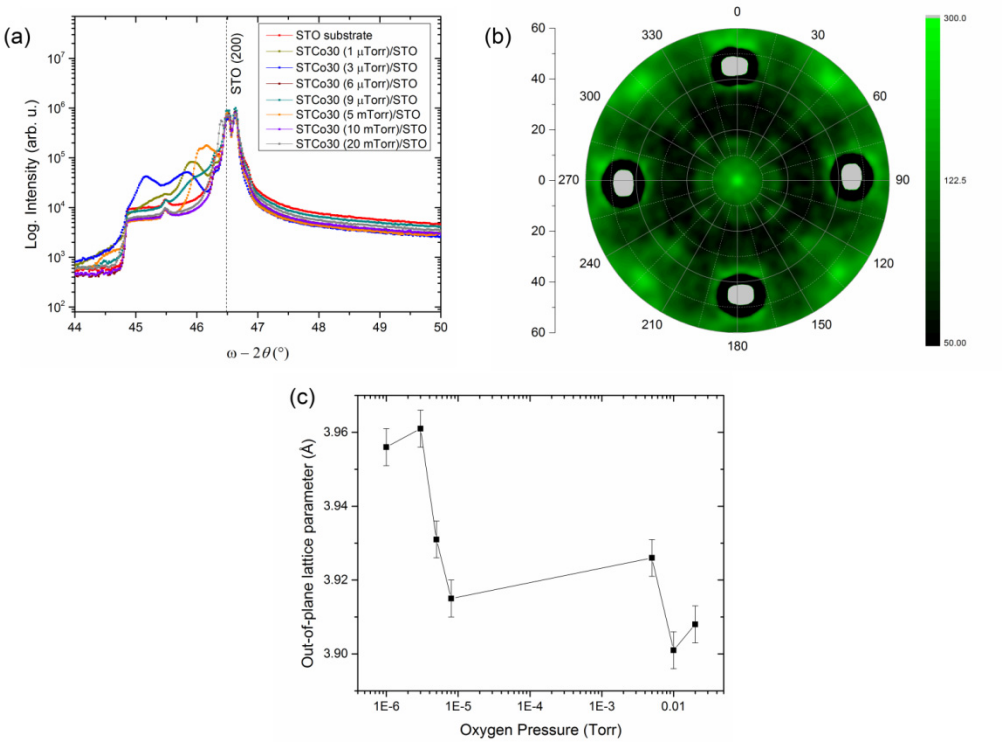

Fig. 1. (a) X-ray diffraction patterns (ω-2θ plots) indicate the phases present for films grown at different oxygen pressures. The strongest peaks are from the STO substrate, as well as a step at 44.8° and a small peak at 45.5°. (b) Two-dimensional XRD scan of 9 μTorr STCo30 film about the 101 peak shows two four-fold symmetric peak sets (0, 90, 180, 270°) and (45, 135, 225, 315°) which correspond to (100) and (111) epitaxial orientations, respectively. The center peak shows 101 oriented crystal. (c) Oxygen partial pressure dependence of the out-of-plane lattice parameters of the films.

For all films, STCo30 (101) and (111) peaks were also observed. This is reminiscent of a similar system, $Sr(Ti,Fe)O_{3-\delta}$, which demonstrated a double-epitaxial microstructure consisting of (100) film containing (110) crystals [17], where each crystal type had a specific orientation with respect to the substrate. A two-dimensional XRD (pole figure) scan about the 101 peak was conducted on the 9 μTorr STCo30 film using the Rigaku Smartlab Multipurpose Diffractometer and In-plane Pole Figure (medium resolution PB) Preinstalled Package in the Smartlab Guidance software. The 9 μTorr STCo30 film was chosen because this sample yielded the strongest STCo (101) peak near 32.4° during the ω-2θ scans. Diffraction angle α was varied from 0° to 90° with a step size of 3° and β was varied from 0° to 360° with a step size of 3° at a speed of 150° per minute. Figure 1(b) displays the pole figure, which shows the cubic four-fold symmetry in the film. The center peak indicates the presence of (101)-oriented STCo30. The set of four peaks at α = 45° correspond to the (111) peaks and indicates the presence of (111)-oriented crystals. The remaining set of four-fold

#234231 - $15.00 USD Received 9 Feb 2015; accepted 30 Apr 2015; published 13 May 2015

symmetric peaks at (0, 90, 180, 270°) indicate the (100)-orientated film. This film therefore had three sets of crystal orientations in the film with specific orientations with respect to the substrate, so could be described as 'triple-epitaxial'. Cross-section transmission electron micrographs (not shown here) obtained for another STCo30 sample on STO (grown at 1μTorr) showed wedge-shaped features nucleating near the film-substrate interface and growing wider as the film thickness increased. These represent crystals other than (100) which are presumed to nucleate to relieve film strain. A more detailed analysis of the thickness dependence of the crystal orientations will be presented elsewhere, but to summarize we believe that the STCo30 films initially grew with cube-on-cube epitaxy on the (100) STO, and the other crystal orientations formed to lower strain as the film grew thicker, leading to the splitting evident in the (200) peak of some of the samples.

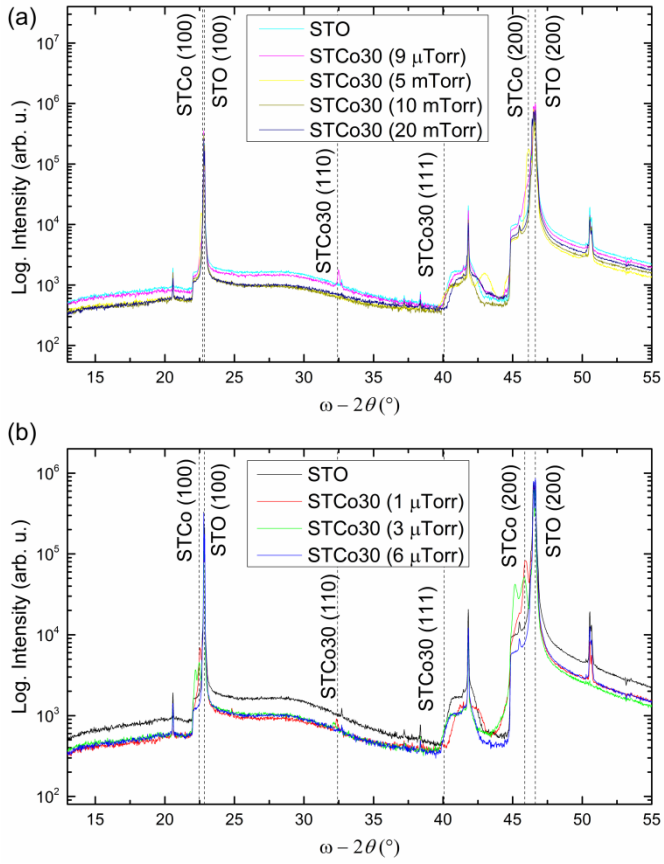

Fig. 2. X-ray diffraction patterns (ω-2θ plots) indicate the phases present for films grown at different oxygen pressures for films grown under (a) 9 μTorr, 5 mTorr, 10 mTorr and 20 mTorr, and under (b) 1, 3 and 6 μTorr. Both plots include the diffraction patterns for bare STO substrate for comparison.

Phases present inside the films are investigated with larger angular range ω-2θ XRD scans as shown in Fig. 2(a) for the 9 μTorr, 5 mTorr, 10 mTorr and 20 mTorr films and Fig. 2(b) for 1, 3 and 6 μTorr films. ω-2θ scans of an STO substrate were included with both plots to distinguish the film and substrate peaks. The peaks without labels originate from the substrate. An XRD reference pattern for a very similar 30 at.% Cobalt-substituted perovskite bulk powder of $SrTi_{0.70}Co_{0.30}O_{2.9}$ (powder diffraction reference number: 00-053-1216) indicates STCo30 (101) and (111) peaks at 2θ = 32.509 and 2θ = 40.078°. All of the peaks are either from the substrate or from the epitaxial film peaks immediately adjacent to the major

#234231 - $15.00 USD Received 9 Feb 2015; accepted 30 Apr 2015; published 13 May 2015

substrate peaks or from the (110) or (111)-oriented perovskite phases, i.e. there were not detectable amounts of other phases.

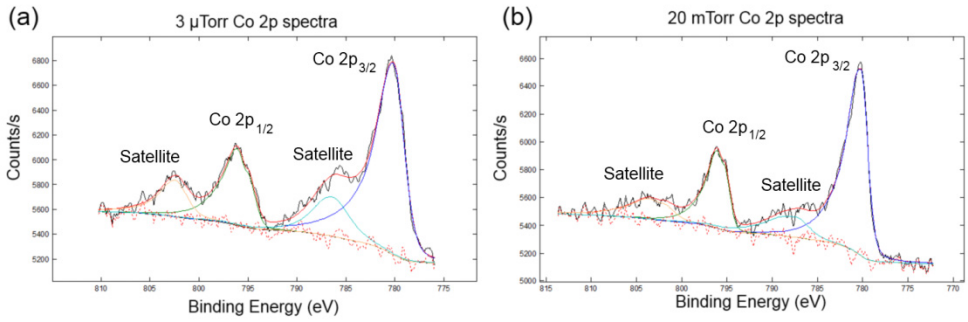

Fig. 3. Cobalt 2p x-ray photoelectron spectra for STCo films grown under (a) 3 µTorr and (b) 20 mTorr oxygen. The Co $2p_{3/2}$ and Co $2p_{1/2}$ doublets for both spectra indicate mixed-valence states for the Cobalt ions.

X-ray photoelectron spectroscopy (XPS) was carried out to investigate the valence states of the cobalt. Figure 3(a) and 3(b) show the XPS spectra for STCo30 (3 µTorr) and STCo30 (20 mTorr) films, respectively. Both spectra show peaks at 780.4 and 796.2 eV, which are the binding energies of Co $2p_{3/2}$ and $2p_{1/2}$ doublets originating from spin-orbit interaction. Cobalt metal is not present according to these spectra, because if metallic Co clusters had formed, the $2p_{3/2}$ and $2p_{1/2}$ peaks would be at 777.3 and 792.4 eV, respectively [3]. The lack of metallic Co peaks in the XRD and XPS spectra indicate that there are no significant amounts of Co metal. Near 786 and 803 eV, the satellite peaks for Co $2p_{3/2}$ and $2p_{1/2}$ doublets are observed. Each satellite peak is 7 eV beyond its principal peak. A 7 eV difference between the principal and satellite peaks is similar to the binding energy differences for Co^{2+} or Co^{3+} ions discussed in previous reports [3]. Typical satellite peaks for Co^{3+} and Co^{4+} ions are weak, as shown for $La_{1-x}Sr_xCoO_3$ [23] and for STCo bulk samples [24] fabricated under high oxygen pressure. In the spectra shown here, the satellite peak is strong, as a characteristic of Co^{2+} ion, as discussed for La_2CoO_4 [25]. The strong satellite peak in the XPS spectrum therefore indicates that the film contains Co^{2+}. In addition, DFT predictions on oxygen-deficient STO with 25% Co substitution, close to the composition of STCo30 [18], also support the presence of Co^{2+}. The binding energy of the Co $2p_{3/2}$ peak is smaller than that of pure Co^{2+} perovskites (781.3 eV) [3], suggesting that Co is in a mixed valence state also containing Co^{3+}. This result is also consistent with the DFT predictions [18]. We therefore believe that Co^{2+} and Co^{3+} are the major valence states of Co within the STCo30 films, both for STCo30 (3 µTorr) and STCo30 (20 mTorr) films. The difference is that in the STCo30 (20 mTorr) film, Co $2p_{1/2}$ peak has lower intensity and hence the Co^{2+} fraction relative to Co^{3+} is lower than in the STCo30 (3 µTorr) film.

Oxygen vacancies are expected to be present for all deposition pressures because $\delta = 0$ would require the Co to be quadrivalent. The reduction in the fraction of Co^{2+} with increasing oxygen partial pressure is expected from a reduction in oxygen vacancy concentration. This also reduces the average size of the Co ion and the lattice volume (assuming $V_{STCo30} = a_{out\text{-}of\text{-}plane} \cdot 3.905^2$ Å^3) as indicated on Table 1. Since earlier studies show that Cobalt is at around 23 at.% [3], the Sr, Ti and Co ionic concentrations are close to those in the the DFT study of STCo [18]. A comparison with DFT results for unit cell volume enables an estimate to be made of the bounds for δ for the films prepared for this study. DFT studies for 25% Cobalt-substituted STO with $\delta = 0$ ($SrTi_{0.75}Co_{0.25}O_3$) and $\delta = 0.125$ ($SrTi_{0.75}Co_{0.25}O_{2.875}$) have unit cell volumes of 57.56 Å^3 and 58.50 Å^3, respectively [18]. The $\delta = 0.125$ case would correspond to Co^{3+} average valence state whereas $\delta = 0.25$ corresponds to Co^{2+} average valence state, with Sr^{2+} and Ti^{4+} present. Since XPS showed that Co^{2+} constitutes a greater fraction of the Cobalt

#234231 - $15.00 USD Received 9 Feb 2015; accepted 30 Apr 2015; published 13 May 2015

ions than Co^{3+}, one can estimate that δ is closer to 0.25 than 0.125. The unit cell volume of all the films is larger than the DFT prediction for δ = 0.125 for all samples, which suggests δ > 0.125 even for films grown in oxygen.

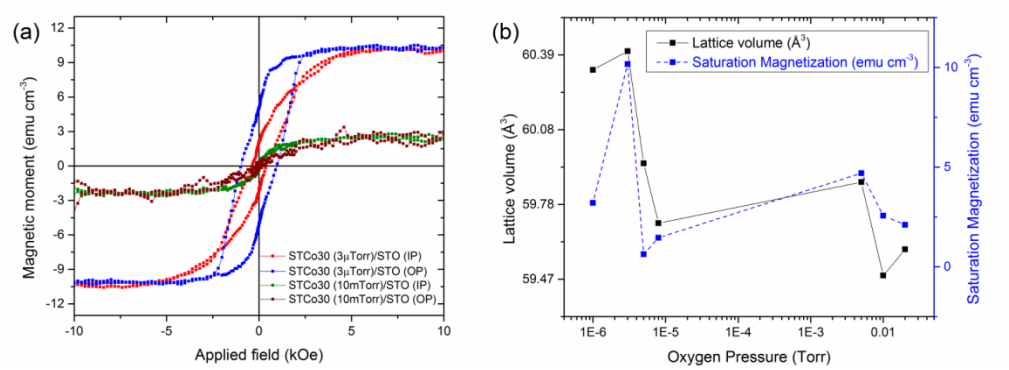

Fig. 4. Oxygen pressure dependence of magnetism and out-of-plane lattice parameter. (a) In-plane and out-of-plane magnetic hysteresis loops of STCo30 (3μTorr) and STCo30 (10mTorr) films. (b) Oxygen partial pressure dependence out-of-plane lattice parameter of the films and saturation magnetization.

In order to investigate how the oxygen partial pressure affects magnetic properties of the films, room temperature magnetic hysteresis loops of the films were measured using a vibrating sample magnetometer (VSM). In the in-plane (IP) hysteresis loops, the magnetic field was oriented and swept parallel to the film surface along the [100] direction. In the out-of-plane (OP) hysteresis loops, the magnetic field was oriented perpendicular to the film surface along [001]. Figure 4(a) indicates the IP and OP hysteresis loops for STCo30 (3 μTorr) and STCo30 (10 mTorr) films. Magnetic saturation moments (M_s) for the films were 10.6 emu·cm^{-3} (~0.23 μ_B/Co ion) and 2.8 emu·cm^{-3} (~0.06 μ_B/Co ion) for STCo30 (3 μTorr) and STCo30 (10 mTorr) films, respectively. Saturation magnetic moments of the films grown at oxygen pressures at or above 6 μTorr were lower than 0.1 μ_B/Co ion, indicating that all of the STCo30 films have a substantial amount of antiferromagnetic coupling between neighboring Co ions. Experimental results on oxygen pressure dependence of M_s are presented in Fig. 4(b) and the M_s shows a strong positive correlation with the lattice parameter. Consistent with DFT predictions [18], increasing oxygen pressure (and decreasing oxygen vacancy concentration) reduces M_s and the lattice volume.

The out-of-plane easy axis evident in the loops of Fig. 4(a) for the 3 μTorr sample is assumed to originate from magnetoelastic anisotropy. With higher oxygen pressure, the films become more isotropic. Octahedrally coordinated Co^{2+} is a highly magnetoelastic ion, and the compressive strain state of the film is assumed to provide magnetoelastic stabilization to align the magnetic moments within the film.

4. Optical and magneto-optical properties of the films

The effect of oxygen pressure during growth on refractive index and extinction coefficient is shown in Fig. 5. Ψ and Δ were measured using a Woollam Vase Spectroscopic ellipsometer. Ψ and Δ are defined as $\tan(\Psi)\cdot e^{i\Delta} = R_p/R_s$. Ψ and Δ are the amplitude ratio and phase difference (in radians) parameters to quantify the change in polarization of an incoming light upon reflecting off the sample surface. R_p and R_s are Fresnel reflection coefficients for the p and s polarizations. The film thicknesses were measured using a KLA Tencor P16 Profilometer. An optical dielectric thin film model of n and k spectra was constructed with Lorentzian oscillators to fit the Ψ and Δ spectra obtained using the ellipsometer. The mean square error in each fit is less than 10^{-3}. The refractive index of the STCo30 films was in the range 2.42 ± 0.03 at λ = 1550 nm, except the 3 μTorr sample has a refractive index of 2.34 at

#234231 - $15.00 USD Received 9 Feb 2015; accepted 30 Apr 2015; published 13 May 2015

λ = 1550 nm, as shown in Fig. 5(a). The lower refractive index is consistent with the presence of the smaller, less polarizable Co^{2+} ions. The optical absorption and extinction coefficients, as shown in Fig. 5(a), generally decreased with higher oxygen pressure. The fits are best around 1550 nm. Figure 5(b) shows optical transmission data for the films as a function of wavelength, from which the band gap can be estimated. Bare STO substrate has an indirect band gap near 3.2 eV (λ_g = 387 nm). STCo30 films have similar indirect band gaps with an absorption tails that extend to longer wavelengths with higher oxygen pressure.

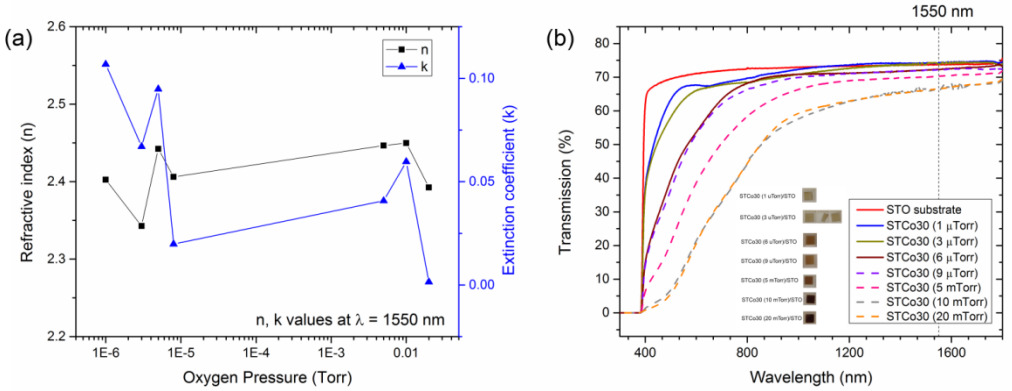

Fig. 5. Optical properties of STCo films. (a) Refractive indices (n) and extinction coefficients (k) at λ = 1550 nm. (b) Transmission spectra of the films (inset: sample photos, in the same order in the legend).

Faraday rotation of the films as a function of applied OP magnetic field was measured using a custom-made setup in transmission mode as shown in Fig. 6(a). Two perpendicularly oriented polarizers placed before and after the sample enabled detection of the rotated electric field intensity using a Ge photodetector. Consistent with the OP magnetic hysteresis loops in Fig. 4(a), Faraday rotation was highest for 3 μTorr film and decreased monotonically with higher oxygen pressure after 3μTorr. The Faraday rotation coercivity (H_c (FR) = 1350 Oe) was greater than that of its OP magnetic coercivity (H_c = 960 Oe) for the STCo30 (3 μTorr) film. The optical loss values on Table 1 were calculated according to the formula: Optical loss (dB) = $-10 \times \log_{10}(\exp(-4\pi k/\lambda_0 \times t))$, where k is the extinction coefficient of the film at 1550 nm, λ_0 is 1550 nm, and t is the film thickness (in nm). The figures-of-merit in Table 1 were calculated as Figure-of-merit = (saturation FR, °·cm^{-1})/(optical loss, dB·cm^{-1}) at 1550 nm.

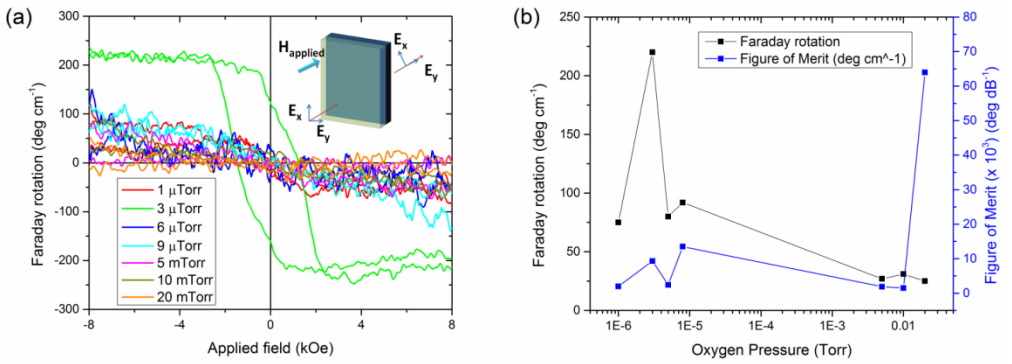

Fig. 6. (a) Faraday rotation loops for each oxygen pressure sample; (b) Oxygen partial pressure dependence of Faraday rotation and Figure-of-merit.

For MO device applications, the optical loss of the films needs to be minimized while maximizing the Faraday rotation. In previous studies of oxides [26], optical loss was higher

#234231 - $15.00 USD Received 9 Feb 2015; accepted 30 Apr 2015; published 13 May 2015

for films with greater Faraday rotation. The figure-of-merit may be optimized by establishing the appropriate oxygen partial pressure window. As shown in Fig. 6(b), Faraday rotation and figure-of-merit results at 1550 nm are plotted as a function of oxygen pressure during growth. Faraday rotation was maximum in the range of 3-9 μTorr, while optical loss was minimum at 20 mTorr. The MO figure-of-merit was numerically greatest near 20 mTorr since the optical loss of the 20 mTorr film was the lowest, but at this pressure the magnetic and MO response of the film is weak. The most plausible choice of pressure was 9 μTorr to provide the best figure-of-merit and magnetization.

The MO figure-of-merit and optical loss values found for STCo30 films and other MO films are listed on Table 2. Other substitutionally-doped STO-based perovskites [3,27] had much higher optical loss near 1550 nm compared with the STCo30 films in this study. The two major categories of MO materials are iron garnets and substitutionally-doped III-V films for non-reciprocal MO devices such as isolators and circulators, in which the figure-of-merit of the MO film needs to reach ~45 °·dB^{-1} [26] and the insertion loss of the device needs to be below ~1-2 dB. Substituted iron garnet films (i.e. Ce:YIG) is often used in non-reciprocal device applications [13, 28–30]. These garnet films have very high MO figure-of-merit in bulk [29,30], but it is lower for integrated thin films [13,28]. Fe-doped group III-V semiconductors also achieve high MO figure-of-merit for devices integrated on a III-V substrate. The STCo30 films presented here have lower figure-of-merit than these two classes of materials, but the perpendicular magnetic anisotropy, which is also seen in polycrystalline STCo30 films grown on Si substrates (not shown here) may have a role in non-reciprocal device architectures requiring perpendicular magnetic anisotropy.

Table 2. Comparison of MO figure-of-merit values for garnets, perovskites and semiconductors.

MO Material and Substrate	MO Figure-of-merit (°·dB^{-1}) near λ = 1550 nm	Growth method	Optical Loss near λ = 1550 nm (dB·cm^{-1})	Other useful properties	Reference
STCo30 (20 mTorr) on STO	0.064	PLD	390.6	Perpendicular magnetic anisotropy	This study
$SrTi_{0.77}Co_{0.23}O_{3-\delta}$ on (001) $LaAlO_3$	0.57	PLD	877	Magnetic up to 1000 K	[3]
$SrTi_{0.6}Fe_{0.4}O_{3-\delta}$ on (001) $LaAlO_3$	1.11	PLD	700	Magnetic up to 1000 K	[27]
$Ce_1Y_2Fe_5O_{12}$ (Ce:YIG) on Silica	56	Sputtering	48	Grown on non-garnet substrate	[28]
Ce:YIG on Si	21.8	PLD	58	Grown on Si waveguide	[13]
$Y_{2.82}Ce_{0.18}Fe_5O_{12}$ (no substrate)	1420	Traveling solvent floating zone	0.52	Bulk crystal	[29]
$Ce_1Y_2Fe_5O_{12}$ on (111) doped-$Gd_3Ga_5O_{12}$	321	Sputtering	14	470-nm thick epitaxial film	[30]
Fe:InP	23.8	(not mentioned)	1.66	III-V semiconductor integration	[31]
Fe:InGaAsP	23	(not mentioned)	4.34	III-V semiconductor integration	[32]

#234231 - $15.00 USD Received 9 Feb 2015; accepted 30 Apr 2015; published 13 May 2015

5. Conclusion

STCo30 films were grown on (100) STO substrates under different oxygen pressures using PLD. The (100) STCo30 films included (110) and (111) oriented crystals assumed to form to relieve strain. As the oxygen partial pressure during growth decreased, the out-of-plane lattice parameters and unit cell volumes increased. Cobalt ions were in mixed valence states (Co^{2+} and Co^{3+}) regardless of oxygen partial pressure during growth, but the ratio of Co^{2+}/Co^{3+} decreased with higher oxygen pressure. The M_s, magnetic anisotropy, and Faraday rotation all decreased with higher oxygen pressure. The decrease in the lattice volumes presented in Table 1 follows trends predicted by DFT calculations of oxygen-deficient structures [18]. The MO figure-of-merit varied with oxygen pressure but was lower than that of iron garnets at 1550 nm. This simple perovskite STCo30 film can be useful in applications requiring perpendicular magnetic anisotropy.

Acknowledgments

This work was funded by the National Science Foundation and FAME, a STARnet Center of SRC supported MARCO and DARPA. MIT Center for Materials Science and Engineering Shared Experimental Facilities has been used, award DMR0819762. TG was supported by a Grant-in-Aid for Young Scientists (A) No. 26706009 and Challenging Exploratory Research No. 26600043.

#234231 - $15.00 USD Received 9 Feb 2015; accepted 30 Apr 2015; published 13 May 2015